



The Vela Pulsar and its Behavioural Variance

A thesis submitted to The Department of Mathematics and Natural Sciences,  
BRAC University, in partial fulfilment of the requirements for the degree of  
Bachelor of Science in Applied Physics and Electronics

Submitted By

Masuda AkterTonima

Applied Physics and Electronics

Department of Mathematics and Natural Sciences

BRAC University

January 2015

## **DECLARATION**

I do hereby declare that the thesis titled “The Vela Pulsar and its Behavioural Variance” is submitted to the Department of Mathematics and Natural Sciences of BRAC University in partial fulfilment of the requirements for the degree of Bachelor of Science in Applied Physics and Electronics. This research is the work of my own and has not been submitted elsewhere for award of any other degree or diploma. Every work that has been used as reference for this work has been cited properly.

MasudaAkteTonima

ID: 11115002

**Candidate**

**Certified**

**(ProfessorMofiz Uddin Ahmed)**

**Supervisor**

Professor

Department of Mathematics and Natural Sciences

BRAC University, Dhaka

## ACKNOWLEDGEMENT

I would like to acknowledge Professor Mofiz Uddin Ahmed who guided me fully throughout the time of my thesis and pushed me until I produced the best results as any good advisor does to prepare their students for future research opportunities.

I also express my gratitude to BRAC University for giving me the opportunity of availing its resources and enhancing my knowledge. The Mathematics and Natural Sciences Department has been supportive in its unique manner— in all academic and official procedures. I am indeed lucky to have an affectionate Chairperson like Professor A.A. Ziauddin Ahmad whose constant guidance and concern had encouraged me to do well in my studies. The fulfilment of the undergraduate studies would not have been possible without the supervision of my course teachers— Mr. Lutfor Rahman, Mr. Mahabobe Shobahani, Dr. Shamim Kaiser, Dr. Md. Firoze H. Haque, Ms. Amel Chowdhury, Ms. Sharmina Hussain, Md. Sazib Hasan, and Mr. Sheik Ahmed Ullah—I am grateful for their effort in making me capable.

## ABSTRACT

This study includes detailed exploration of Vela pulsar magnetosphere and glitches—including recent studies that compare Vela pulsar with other pulsars such as: PSR B0329+54, an optical pulsar (the Crab pulsar, PSR B0531+21), an old millisecond pulsar (PSR J0437-4715) and the 2<sup>nd</sup> fastest known pulsar (PSR B1937+21). The explored energy band shows  $\gamma$ -ray to be the strongest in emission. Its helical structure and magneto-dynamic instability give further insight to this. Exploration of the magnetosphere shows the effect of pair production and gap on Lorentz factor that is balanced between electric and radiation reaction force—and how that is affected within a boundary. We further explore the magnetosphere in terms of X-ray field, curvature radiation-outside the gap, electric structure,  $\gamma$ -ray spectrum and spectral dependence on the curvature of field line to understand Vela pulsar better. This, we combine with Gvaramadze's study to prove the relationship of the pulsar velocity with distance.

# CONTENTS

## Table of Contents

<b>DECLARATION</b> .....	<b>II</b>
<b>ACKNOWLEDGEMENT</b> .....	<b>III</b>
<b>ABSTRACT</b> .....	<b>IV</b>
<b>CONTENTS</b> .....	<b>V</b>
<b>LIST OF FIGURES</b> .....	<b>VII</b>
<b>LIST OF TABLES</b> .....	<b>IX</b>
<b>CHAPTER 1: DISCOVERY OF THE VELA PULSAR</b> .....	<b>1</b>
1.1 HISTORY BEHIND DISCOVERY .....	1
1.2 DISCOVERY OF VELA PULSAR: .....	2
<b>CHAPTER 2: POSITION AND PHYSICAL STRUCTURE OF VELA PULSAR</b> .....	<b>4</b>
2.1 CHARACTERISTICS: .....	5
2.2 VELA PULSAR DYNAMICS: .....	7
2.2.1 <i>Helical structure—precession</i> : .....	10
2.2.2 <i>Kink magneto-hydrodynamic instability</i> : .....	12
<b>CHAPTER 3: CHARACTERISTICS OF VELA PULSAR</b> .....	<b>14</b>
3.1 COMPARISON WITH OTHER PULSARS: .....	14
3.2 FURTHER EXPLORATION OF THE GLITCH: .....	18
3.2.1 <i>Starquake model for vela</i> :.....	19
3.2.2 <i>Vortex unpinning for Vela</i> : .....	20
3.3 PWN STUDY OF THE VELA: .....	28
<b>CHAPTER 4: MAGNETOSPHERE OF VELA PULSAR</b> .....	<b>29</b>
4.1 BOUNDARY .....	30
<b>CHAPTER 5: PULSAR MAGNETOSPHERE ELECTRODYNAMICS</b> .....	<b>32</b>
<b>CHAPTER 6: EXPLORING VELA PULSAR MAGNETOSPHERE</b> .....	<b>34</b>
6.1 X-RAY FIELD: .....	34
6.2 CURVATURE RADIATION-OUTSIDE THE GAP:.....	34
6.3 THE ELECTRIC STRUCTURE: .....	35
6.4 GAMMA-RAY SPECTRUM:.....	36

6.5 SPECTRAL DEPENDENCE ON THE CURVATURE OF FIELD LINE: .....	37
<b>CHAPTER 7: GVARAMADZE'S STUDY ON THE VELA PULSAR.....</b>	<b>38</b>
7.1 VELOCITY OF VELA PULSAR: .....	38
<b>DISCUSSION.....</b>	<b>40</b>
<b>BIBLIOGRAPHY .....</b>	<b>41</b>

## LIST OF FIGURES

FIGURE 1 PULSE PROFILES OF THE VELA PULSAR IN THE RADIO, OPTICAL, X-RAY AND $\Gamma$ -RAY REGIME [10] .....	5
FIGURE 2 THE SPECTRUM OF THE VELA PULSAR FROM PEV TO GEV [11] .....	6
FIGURE 3 THREE 2009 DATA- PROJECTED TRACE OF THE BEST-FIT HELICAL MODEL SUPERIMPOSED (GREEN). THE ENVELOPE AND GUIDING LINE ARE MARKED AS DOTTED AND DASHED BLUE LINES. BLACK X-MARK SHOWS THE LOCATION OF THE PULSAR AND A WHITE VECTOR SHOWS THE DIRECTION OF PROPER .....	8
FIGURE 4 EIGHT OF THE 2010 DATA, TAKEN FROM JUNE TO SEPTEMBER. THE PARAMETERS ARE SAME AS ABOVE. ....	8
FIGURE 5 DIFFERENCE BETWEEN THE FIRST AND LAST OBSERVATIONS IN 2010. THE INNER JET- BLUE DOTTED LINE, PULSAR POSITION—BLUE CIRCLE, ARC POSITION IN 1ST IMAGE—DARK REGION WITH GREEN DASHED LINE, ARC POSITION LAST IMAGE—BRIGHTER REGION WITH CYAN DASHED LINE, THE ARROWS POINT TOWARDS THE APPARENT MOTION FOR BOTH ARC AND JET [12] .....	11
FIGURE 6 COMPARISON BETWEEN THE EMISSIONS OF VARIOUS PULSARS [13]. .....	14
FIGURE 7 THE COMPARISON .....	16
FIGURE 8 THE COMPARISON OF THESE SEVEN PULSARS PLOTTED AS $\log F_V$ AGAINST $\log V$ (LOG ENERGY IN KEV) [6].....	16

FIGURE 9 THE OBSERVED PULSAR LUMINOSITIES PLOTTED AGAINST THE ESTIMATED GOLDREICH-JULIAN CURRENT OF HIGH-ENERGY PARTICLES [6] .....17

FIGURE 10 THE RELATIONSHIP OF THE PREDICTED TIME OF GLITCH AND GLITCH SIZE. FOR VELA - THE RED LINE IS THE LINEAR FIT PASSING THROUGH ORIGIN TO ALL DATA AND THE CYAN LINE IS THE BEST-FITTED LINE FOR THE LARGE GLITCHES; HOWEVER, NO SUCH RELATIONSHIP IS OBSERVED FOR THE LARGE GLITCHES; HOWEVER NO SUCH RELATIONSHIP IS OBSERVED FOR CRAB [18].....25

FIGURE 11 THE SUM OF GLITCH MAGNITUDE VERSUS TIME PLOTTED FOR VELA AND CRAB. THE SLOPE GIVES THE VALUE OF GLITCH ACTIVITY,  $A_G$ , WHICH FOR THE VELA PULSAR IS APPROXIMATELY  $8 \mu\text{HZ}/\text{YR}$  [18].....25

FIGURE 12 THE PLOTTED CUMULATIVE DISTRIBUTION FUNCTION (CDF) AND NORMAL DISTRIBUTION FUNCTION PLOTTED AND COMPARED WITH EACH OTHER [18].....26

FIGURE 13 COMPARISON OF THE CUMULATIVE DISTRIBUTION FUNCTION (CDF) WITH THE NORMAL AND POISSON DISTRIBUTION FUNCTION, ENABLING THE DETERMINATION OF THE CONCLUSION, I.E. THE DISTRIBUTION OF GLITCHES IN TIME IS NOT RANDOM FOR VELA. [18]....26

FIGURE 14 DISTANCE (ALONG THE FIELD LINES) VERSUS ELECTRIC FIELD....36

FIGURE 15 843 MHZ IMAGE OF THE CENTRAL PART OF THE VELA SNR, THE POSITION OF THE VELA PULSAR IS INDICATED BY THE CROSS MARK. THE ARROW ATTACHED TO IT SHOWS THE DIRECTION OF THE PULSAR PROPER MOTION VELOCITY [21] .....39



## LIST OF TABLES

TABLE 1.1 THE DISSIMILARITIES OF THE VELA PULSAR WITH 7 OTHER PULSARS [9]:.....	14
TABLE 2 THE DATA USED FOR THE RELATIONSHIP CURVES ARE THUS GIVEN.....	24

## CHAPTER 1: DISCOVERY OF THE VELA PULSAR

### 1.1 History behind Discovery

Most scientists were reluctant in accepting the existence of such a thing even though the model of neutron stars were provided by Oppenheimer and Volkoff as early as 1939—who suggested that a neutron star was an ideal gas of free neutrons. Being extremely heavy particles by themselves, neutrons can account for the heavy mass of the neutron stars ( $\sim 10^{14}$  g/cm<sup>3</sup>).

It is believed that pulsars were finally discovered because of World War II—the remnant radio technology of the war allowed astronomical observations of such phenomenal celestial beings to be discovered. Sir Anthony Hewish with a group of research students began the expedition for pulsars in 1967 at the Cambridge Radio Observatory—they surveyed low frequencies around 81 MHz emitted from sources outside the Milky Way Galaxy—sources that scintillated plasma while propagating in space. The signal charts showed periodic disturbances, that Jocelyn Bell carefully studied and, confirmed that that its origination from beyond the solar system. This was the first ever, recorded study of pulsars—and Jocelyn Bell Burnell (even though excluded from the much-deserved Nobel Prize) is known as the astrophysicist who discovered the first radio pulsar.

## 1.2 Discovery of Velapulsar:

The study Jocelyn Bell Burnell by leads us to the question of 'what is a pulsar'?The remnants of a massive supernova collapse to form a dense neutron star—conservation of initial angular momentum causes its rotational speed to increase significantly.i.e.  $L = mvr$ , since  $L$  is constant,  $m$  is constant and  $r$  decreases,  $v$  must increase in order for conservation to occur. When these neutron stars emit detectable radiation once per rotation, it is called as a pulsar. There are various kinds of emission of beams made by a pulsar that originates due to the misalignment of rotational axis with its magnetic field [1]. Classifying a pulsar depends on its specific type of emission, pulsation period, spin down age etc. The primary types of pulsars are:

1. Radio or Rotation- powered pulsar: loss of rotational energy cause gain in power.
  - a. Millisecond pulsar
2. X-ray or Accretion-powered pulsar: gravitational potential energy of the accreted mass account for the power of the X-ray emission.
  - a. High-mass X-ray binaries (HMXB)
  - b. Low-mass X-ray binaries
  - c. Millisecond pulsar
3. Magnetar: decay of strong magnetic field accounts for power gain. (100 to 1000 times stronger than radio pulsars)
  - a. Anomalous X-ray Pulsar
  - b. Soft gamma repeater

- c. Radio pulsars with flat spectrum (XTE J1810-197) (noted as an exceptional case).
- 4. Optical pulsar: rare form of visible pulsar (e.g.: Crab)
- 5. Gamma-ray pulsar: young neutron stars with strong magnetic fields (e.g. Geminga).

Soon after the discovery of the first radio pulsar in 1967, PSR B0833—45 was discovered by the astronomers Large, Vaughan and Mills of the University of Sydney in 1968. This discovery was made during a general search for pulsars using a technique that was designed to detect single pulsars in the southern sky. The pulsar showed such strong characteristics in terms of individual pulses that the periodicity was immediately determinable by the astronomers; i.e., 89 ms—the shortest pulsation period of any pulsar that was known at that time.

## CHAPTER 2: POSITION AND PHYSICAL STRUCTURE OF VELA PULSAR

The discoverers found that the pulsar in question is located at the centre of the Vela Nebula, a supernova remnant that is  $4^\circ$  or  $5^\circ$  in diameter. This nebula was already well known for radio emission. The PSR B0833—45 was soon after identified as a rotating neutron star that originated from the centre of a supernova explosion.<sup>1</sup>The G263.9-3.3 supernova remnant i.e. the Vela SNR is the closest composite SNR containing an active pulsar at its centre from the Earth (at a distance of 290 pc or 945.9 ly); this allows greatly detailed study of its electromagnetic emissions.

The Vela SNR is well known also for its hosting of several dependent pulsars, non-thermal or diffuse radio emission labelled, such as the Vela-X, Vela-Y and Vela-Z [2]. The brightest of them all is the Vela-X pulsar Wind Nebula (PWN) that has a puzzling double arc structure and spans over a region of  $2^\circ \times 3^\circ$  around the pulsar—that has its brightest radio filament at  $45' \times 12'$  south of the Vela Pulsar [3].

---

<sup>1</sup> This centre was not the centre of the visible remnant, rather the centre of the remnant that included other radiations that extended further and were invisible to the naked eye [ 4].

## 2.1 Characteristics:

Even though initially the Vela pulsar was identified as a radio-emitting pulsar [5], its pulsations were later detected in high-energy (HE)  $\gamma$ -rays [6], Optical [7] and X-rays [8]. With a spin down age of  $\tau = 11$  kyr, spin down power  $E = 7 \times 10^{36}$  erg  $s^{-1}$  and unvaried pulsation of  $P = 89$  ms—the  $\gamma$ -ray observation by Fermi Large Area Telescope (LAT) confirms detection above 20 MeV, allowing extended study on the properties of such waves that expose magnetospheric emission over 80% of the pulsation period. Of all the types of emission of the pulsar  $\gamma$ -ray is the strongest where optical and X-ray is barely detectable [9], the figure 2.1a,  $E^2 \frac{dF}{dE}$  versus  $E$ —the HE spectrum over power in average time shows that majority of the emitted energy falls under the  $\gamma$ -ray region rather than the optical or X-ray.

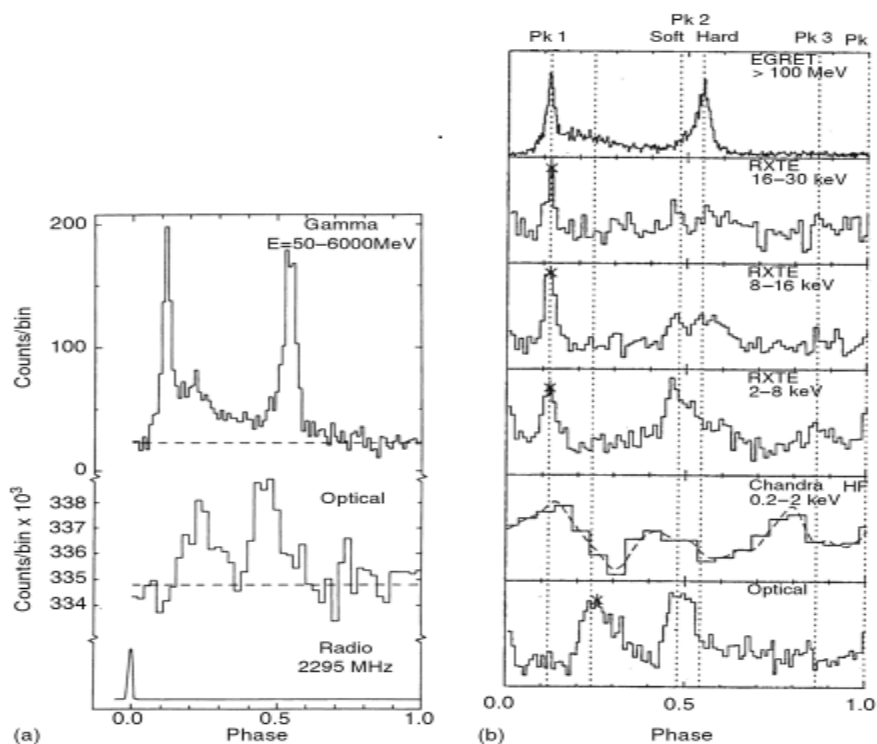
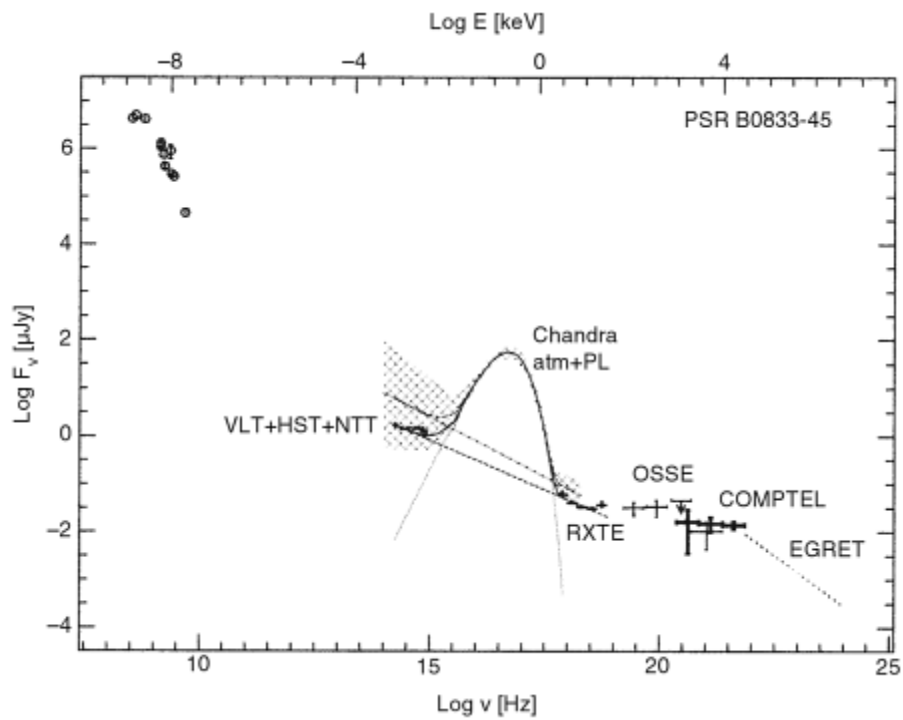


Figure 1 Pulse profiles of the Vela pulsar in the radio, optical, X-ray and  $\gamma$ -ray regime [10]

Figure 2 on the other hand shows the overall spectrum with average phase of the Vela pulsar indicating few important components[9]:<sup>2</sup>

- i. Radio spectrum of spectral index of -2.4
- ii. Radio spectrum of a low frequency turnover of approximately 600MHz
- iii. Continuous spectrum from IR trough visible, X-ray to  $\gamma$ -ray
- iv. Thermal radiation from neutron star surface that dominates the soft X-ray source.



**Figure 2 The spectrum of the Vela pulsar from peV to GeV [11]**

<sup>2</sup>Some of these components resemble components of the crab pulsar in the crab nebula [5].

## 2.2 Vela pulsar dynamics:

Generally, the rapid rotation of a pulsars magnetosphere is responsible for its particle acceleration, electric field and pulsed radiation across the electromagnetic spectrum. The confined formation of the rigidly structured jets caused due to pulsar spin and PWN structures (like the Vela PWN) has been studied in details to explore the implications in MHD instability scenarios etc[12].

After observing the Vela Nebula with advanced CCD Imaging Spectrometer (ACIS) via the Chandra X-ray Observatory, three observational studies have been penned down which were performed in July 2009 and eight more from June 2010 to September 2010. These observations were allotted an exposure time of 40ks with intervals of 7 days between them. The mode used for this observation was FAINT telemetry mode with a frame time of 3.24s. The observation showed no part of red-out streak (due to the bright pulsar) overlapping with the jet. Ignoring energy band of 0.5 to 8 keV, with standard filtering and with parameters of  $\tau = 122$ days,  $\lambda = 0.23$  ly and  $\theta = 10^0$ , the following images were observed [12].



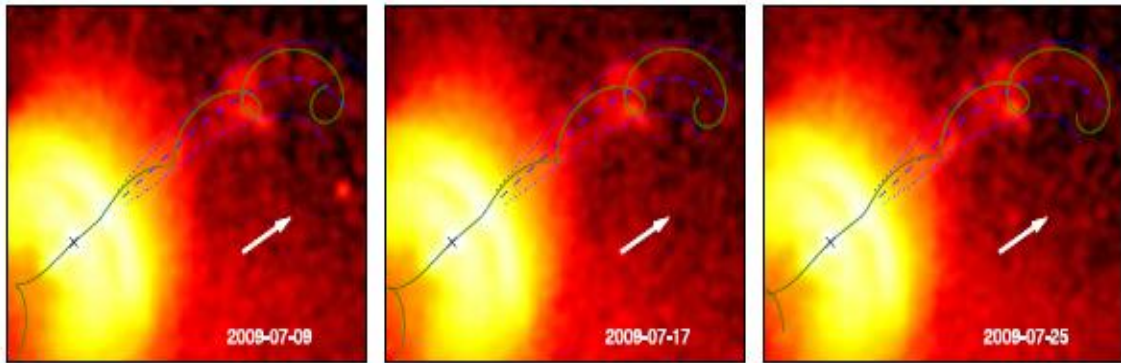


Figure 3 Three 2009 data- projected trace of the best-fit helical model superimposed (green). The envelope and guiding line are marked as dotted and dashed blue lines. Black X-mark shows the location of the pulsar and a white vector shows the direction of proper motion

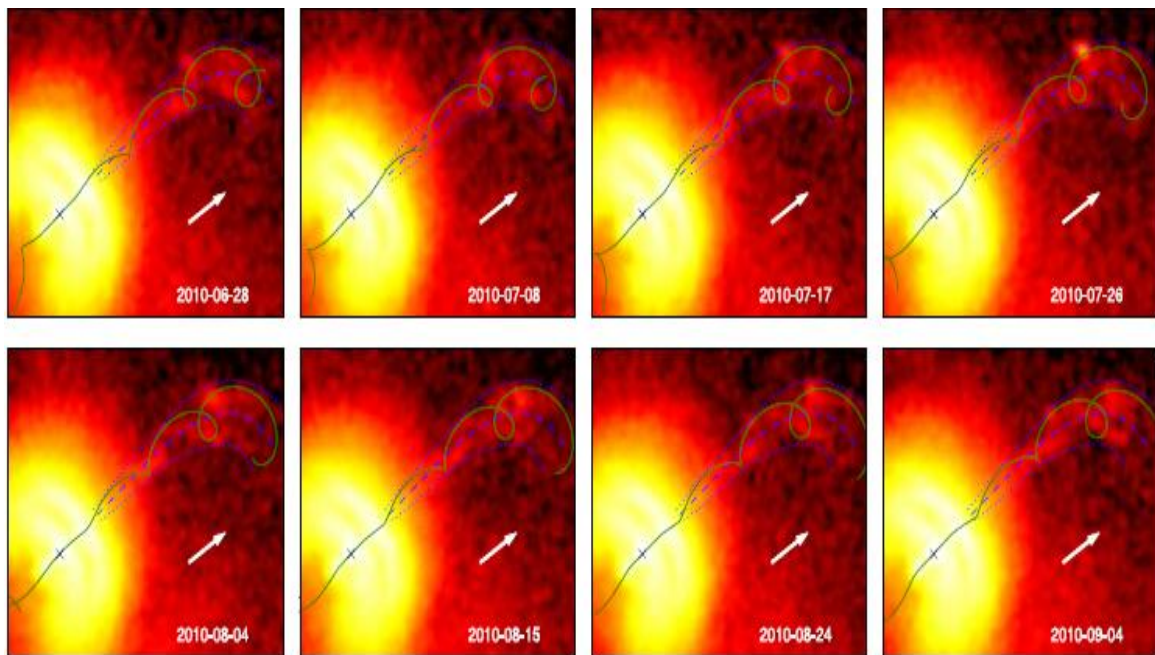


Figure 4 Eight of the 2010 data, taken from June to September. The parameters are same as above.

Two components of the jet were observed in the direction of the pulsar proper motion—

- i. The bright inner jet—that extends for approximately 13” from the pulsar to the outer arc of the pulsar wind nebula.
- ii. The outer jet—less bright yet extends approximately another 100”.

Regardless of the changing shape, the jet as a whole can be seen to be of a well-defined shape that is called the envelope, though initially is narrow and only pointing towards the pulsar’s proper motion, gradually bends the opposite way at greater distances from the pulsar. The brighter inner jet does not show much motion and the outer jet emerges beyond the outer arc – this resembles a simple geometrical model where a small perturbation propagates to a point where the result is a three-dimensional helix. A helical structure is generally seen in AGN jets, protostars and accreting binary systems. Most frequently mentioned of the possible mechanisms leading to a helical structure is the helical instability mode in a magnetized plasma column or jet precession [12]. In an Active Galactic Nucleus jet model the involved precession is torque-driven via interactions between the accretor and the accretion disk. magneto-hydrodynamic (MHD) instability, as an alternative scenario, does not require any external force; instead, the helical pattern grows from a small perturbation, which may be any random fluctuation.

Durant [12] discusses the implications of this three-dimensional helical structure caused due the ballistic flow. For the Vela pulsar, Durant [12] considers only two mechanisms that are more probable to have given rise to the helical structure:

- i. Free precession, that is independent of external torque [torque driven is not considered due to lack of evidence of accretion or a companion].
- ii. Kink magneto-hydrodynamic (MHD) instability in the jet flow.

### 2.2.1 Helical structure—precession:

After various conclusions that were failed to be proven on the basis of precession, a relationship between the precession period,  $\tau$  and the spin period  $P$  was established by Popov in 2008 i.e.  $\tau \sim k P^{1/2}$ , according to which  $\tau$  for Vela is 120 days. Similarly, Jones calculated a correlation between the long-term period and the pulsation period, which is again due to precession. According to this calculation, pulsars with periods of 80-200 days range have a pulsation period  $P$  of 89 ms. Therefore it is quite possible that the Vela pulsar jet's helical shape is due to free precession. In such a case, the long-term radio should have been able to detect it; however, the glitching behaviour of the pulsar complicates the study. With the reference to the following formula for theoretical implication:

$$\epsilon = \frac{I_3 - I_1}{I_1} \quad (1)$$

$$\epsilon = \frac{P_{spin}}{P_{prec}} \quad (2)$$

$$\epsilon \approx 8 \times 10^{-9},$$

Where  $I$  is the moment of inertia, Durant [12] sets a limit on the amount of mass in the super-fluid interior. Instead of dampening the precession, the core partially participates in it. "Indeed, Popov (2008) suggests that glitching—exchange of angular momentum between the crust and the core—can actually be the excitation mechanism for precession" [12].

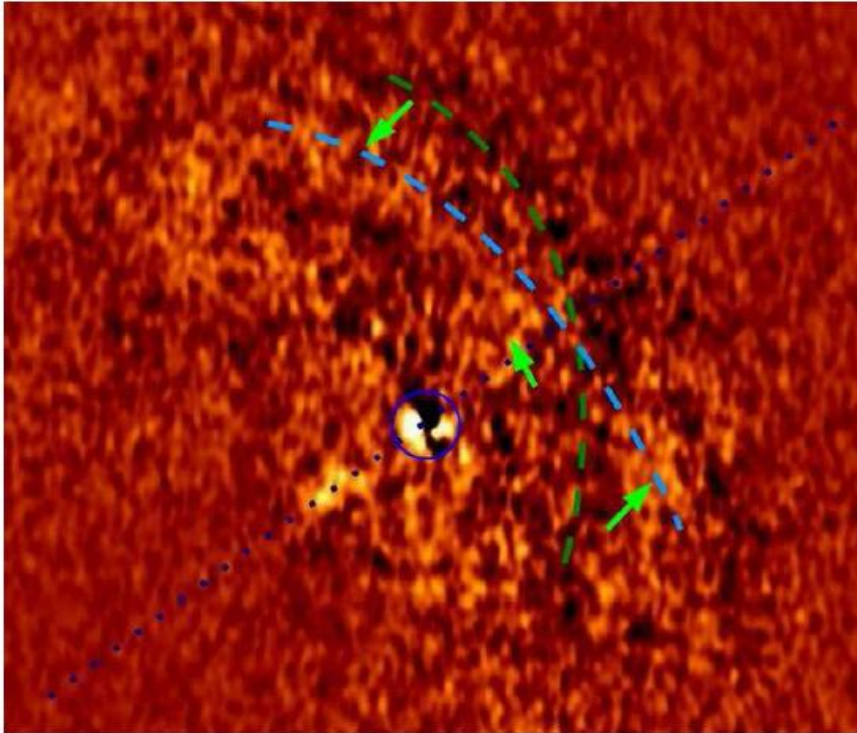


Figure 5 Difference between the first and last observations in 2010. The inner jet—blue dotted line, pulsar position—blue circle, arc position in 1st image—dark region with green dashed line, arc position last image—brighter region with cyan dashed line, the arrows point towards the apparent motion for both arc and jet [12]

The figure 5 (above) shows, the change of path throughout 2010, which Durant [12] concludes as a viable explanation for precession being a ‘natural candidate’ for being reasonable for the formation of helical jets.

### 2.2.2 Kink magneto-hydrodynamic instability:

Durant [12] suggests that despite the model of jet being strictly periodicity built-in, it may still resemble the outcome of kink if the initial perturbation is kosher. Durant [12] brings in Hardee's argument of numerical simulations of the kink instability in the non-linear regime being able to produce helix like structures, with current, sheer velocity or jet precession mechanisms being possible drivers of the kink; then concludes that the relation of period,  $\tau$  of the helical model with the characteristic timescale of the appearance of successive kink cannot be truly periodic unless the trigger is in precession.

He again argues the from AGN perspective—the studies that show that the instability growth timescale for the global kink development can be roughly estimated as-

$$t_i \sim \frac{R_{jet}}{V_A}, \quad (3)$$

Where  $R_{jet}$  is the jet radius and  $V_A$  is the Alfvén speed. ( $R_{jet} \approx 5''$  and  $V_A = 0.77c$ ), therefore:

$$t_i \sim 100 \text{ ds},$$

The distinct helical patterns in figures 3 and 4 can be seen to be emerging from a distance of  $d_i \sim 1'$  from the pulsar, from which Durant [12] derives the approximation for flow velocity:

$$\frac{d_i}{t_i} \sim 0.9 c.$$

Assuming that the start of instability is at much smaller distance from the core than the emerging distance,  $d_i$ .

For exceptional cases such as the extreme bending observed in February of 2000 [12], larger instability timescale should be observed compared to the estimated value. For which Durant [12], concludes that precession is a better explanation than kink MHD. However, factors causing delay in nonlinear instability in growth may be present which may cause problems in calculation. Pulsar jet behaviour may also be hampered by ram pressure at large distance.<sup>3</sup>

Since the trial-error based study does not confirm anything for Durant [12], they conclude that further study of reason behind Vela pulsar jets' structures can result into Vela pulsar being the best persistent sources of gravitational waves.

---

<sup>3</sup> This affect by ram pressure is due to the combined action of the pulsar's motion and a strong wind within the SNR, possibly caused by the passage of the reverse shock, moreover the ram pressure can explain the clockwise bending of the jet's end and the distortion of the helical structure at large distances from the pulsar [12].

## CHAPTER 3: CHARACTERISTICS OF VELA PULSAR

### 3.1 Comparison with other pulsars:

The Vela pulsar despite initially being categorized as a radio emitting pulsar resemble old/new neutron stars, anomalous X-ray pulsars, and young radio pulsars, even though their pulsation periods are way beyond similar; the differences with the same kinds are also present. The figure below shows the comparison (of the emission graphs) between a typical pulsar (PSR B0329+54), the Vela pulsar (PSR B0833-45), an optical pulsar (the Crab pulsar, PSR B0531+21), an old millisecond pulsar (PSR J0437-4715) and the 2<sup>nd</sup> fastest known pulsar (PSR B1937+21):

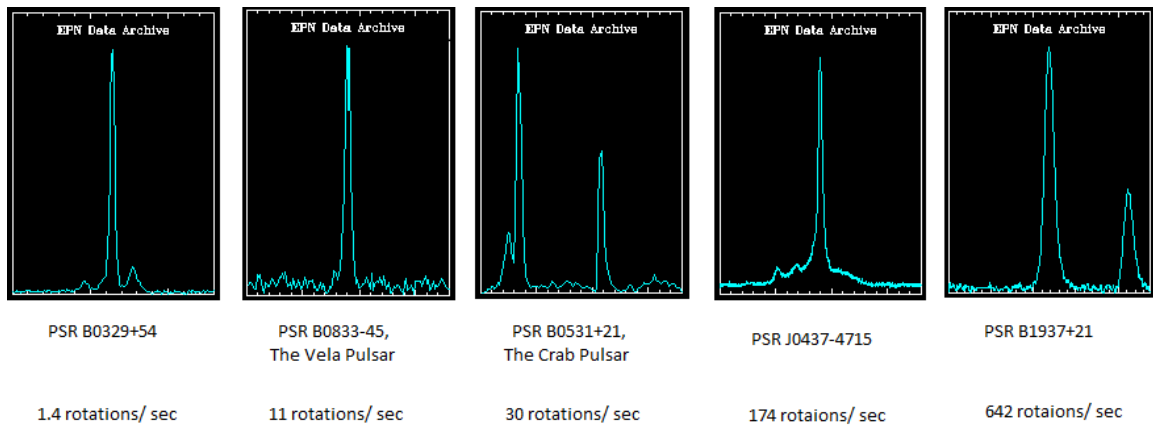


Figure 6 Comparison between the emissions of various pulsars [13].

Table 1.1 The dissimilarities of the Vela pulsar with 7 other pulsars [9]:

PSR names	P in ms	$\dot{E}_{rot}$ erg s <sup>-1</sup>	$\dot{E}_{obs}$ erg s <sup>-1</sup>	Efficiency $\eta \times 10^{-2}$	$N_{GJ}$ s <sup>-1</sup>
B0531+21	33.4	$4.5 \times 10^{38}$	$5 \times 10^{35}$	0.1	$1.7 \times 10^{34}$

(Crab)					
<b>B0833-45</b> (Vela)	89.3	$7 \times 10^{36}$	$2.4 \times 10^{34}$	0.34	$2.1 \times 10^{33}$
<b>J0633+1746</b> (Geminga)	237	$3.3 \times 10^{34}$	$9.6 \times 10^{32}$	2.9	$1.5 \times 10^{32}$
<b>B1706-44</b>	102.5	$3.4 \times 10^{36}$	$6.9 \times 10^{34}$	2.0	$1.5 \times 10^{33}$
<b>B1509-58</b>	150.7	$1.8 \times 10^{37}$	$1.6 \times 10^{35}$	0.9	$3.4 \times 10^{33}$
<b>B1951+32</b>	39.5	$3.7 \times 10^{36}$	$2.5 \times 10^{34}$	0.7	$1.5 \times 10^{33}$
<b>B1055-52</b>	197.1	$3 \times 10^{34}$	$6.2 \times 10^{33}$	21	$1.4 \times 10^{32}$

As mentioned by Lyne & Smith [9] the population of pulsars within a Galaxy requires a model where their luminosity depends upon its rotation rate; the simplest approach is thus mentioned as luminosity being proportional to spin down energy and its power,  $\dot{E}$  &  $\dot{E}^{\frac{1}{2}}$  respectively. “[14]Pointed out that such a power law cannot extend to young pulsars, which are no more luminous than many middle-aged pulsars” [9]—thus inefficient in converting spin down energy to radio power.



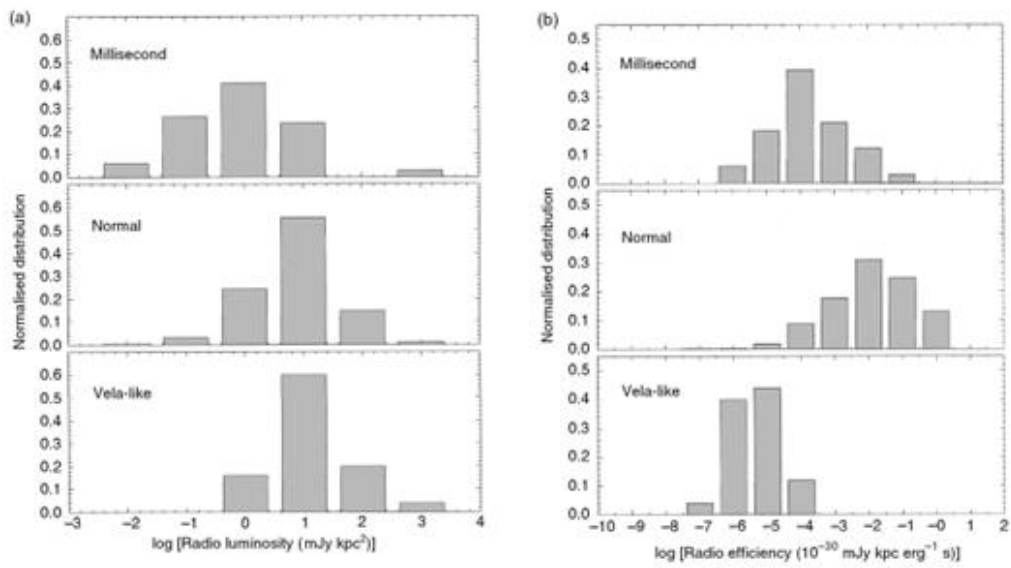


Figure 7 The comparison

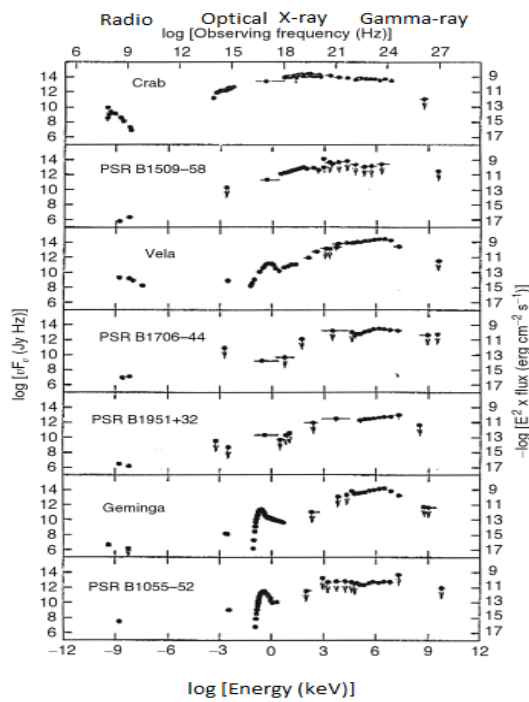


Figure 8 The comparison of these seven pulsars plotted as  $\log \nu F_\nu$  against  $\log \nu$  ( $\log$  energy in keV) [6].

The total emitted power,  $\dot{E}_{obs}$  can be derived from the data of the listed pulsars in fig 8 from which, for conventional parameters,  $\dot{E}_{rot}$  (spin down luminosity) can be written as [9]:

$$\dot{E}_{rot} = 3.95 \times 10^{31} \left( \frac{\dot{P}}{10^{-15}} \right) (P_{sec})^{-3} \text{ erg s}^{-1} \quad (4)$$

Where  $\dot{E}_{rot} \propto \dot{P} P^{-3}$  &  $\dot{E}_{obs} \propto \sqrt{\dot{P} P^{-3}}$

Lyne & Smith [9], express voltage drop in magnetosphere or rate of particle outflow over polar cap as possible reasons behind the oddity of the two relationships. Assuming  $B_{12}$ , the polar magnetic field in the parameter of  $10^{12}$  gauss, they further derive the relation of particle outflow rate,  $\dot{N}_{GJ}$  with the Goldreich-Julian density,  $n_{GJ}$  and polar cap area,  $A_{pc}$  [9]:

$$\dot{N}_{GJ} = n_{GJ} A_{pc} \simeq 1.4 \times 10^{38} \dot{P}^{\frac{1}{2}} P^{-\frac{3}{2}} \text{ s}^{-1} \quad (5)$$

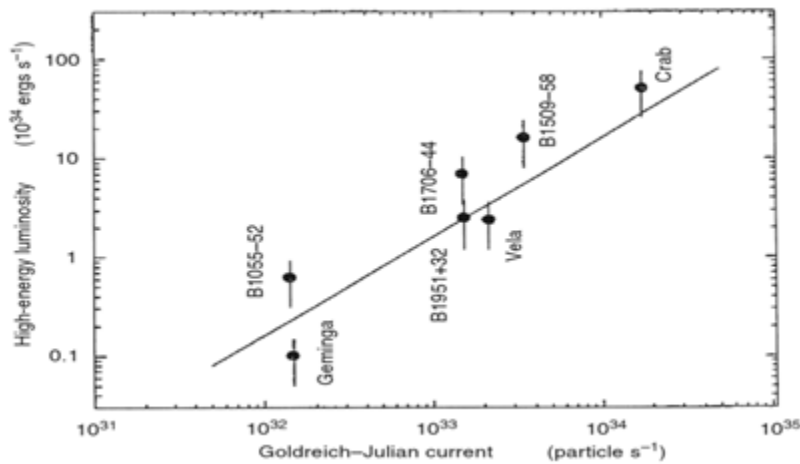


Figure 9 The observed pulsar luminosities plotted against the estimated Goldreich-Julian current of high-energy particles [6]

Hence, the overall efficiency mentioned in Table 1 is seen to be ranging quite widely from 0.001 to 0.207 for the listed pulsars. Where the relationship of the  $\dot{E}_{obs}$  &  $\dot{N}_{GJ}$  is seen quite close—showing the existence of direct relationship of emission with HE particle flux. However, this relationship vanishes in the lower part of the electromagnetic spectrum. This causes Lyne & Smith [9] to suggest this as the direct link between magnetospheric dynamics and observed parameters.

The Vela pulsar has displayed some similarities with some AXP's and SGR's as well. A recent paper [15] has explored these extraordinary similarities with magnetars; this takes into account the activities of (AXP) 4U 0142+61, AXP 1RXS J170849.0–400910, the Vela pulsar, and other radio pulsars for a period of 5 years (1994 – 1999). The study includes observation of activities, time analysis, pulsation analysis etc. to form comparative profiles, showing a significant increase in frequency ( $\Delta\nu/\nu$ ) which results in increase in spin down rate to be:  $\frac{\Delta\nu}{\nu} = (1.4 \pm 0.5) \times 10^{-2}$  [14]. The conclusion is drawn for all of these pulsars to have shown similarities in frequency jumping that can be only categorized a glitch—since this behaviour has not been seen in any other pulsar before.

### **3.2 Further exploration of the glitch:**

Negi [16] thinks glitches of a neutron star yield important information about its origin and structure. The two mainly accepted models of such are:

- i. The starquake model
- ii. The vortex-unpinning model.

The starquake model as the name suggests - refers quakes occurring in the stars that are analogous to earthquakes, interfering with the physical characteristics of the neutron star. Duncan and Thompson [17] suggest in their paper the possibility of these quakes to be the source of giant gamma ray flares. The cause of starquakes can either be:

- i. Stress (caused by kinks in the magnetic fields) exerted on the surface of the neutron star,
- ii. Spindown.

Similarly the vortex unpinning model is as the name suggests, refers to unpinning and displacement of vortices that connect the crust with the superfluid core.<sup>4</sup>

Negi [16] mentions that both the models are dependent on same conventions of neutron stars being two component structures: one, consisting of a super-fluid interior consisting of the maximum mass of the star [previously mentioned in this paper], which is surrounded by the, second, minimal massed thin crust.

### **3.2.1 Starquake model for vela:**

According to the starquake model, the fractional moment of inertia or better articulated as the Vela pulsars glitch-healing parameter is expressed as the ratio of the moment of inertia of the superfluid core to the moment of inertia of the entire mass, i.e.

$$Q = \frac{I_{core}}{I_{total}} \quad (6)$$

---

<sup>4</sup> These data have been gathered from the Astronomy Magazine.

The average of 11 measurements show  $Q = 0.12 \pm 0.7$ , while estimates agree with a range of  $Q \leq 0.2$ . Hence, Negi [16] mentions Vela pulsar to be inconsistent with the starquake model since implied mass of Vela ( $\leq 0.05 M_{\odot}$ ) is too low compared to the mass of a general neutron star.

### 3.2.2 Vortex unpinning for Vela:

The detailed model for the Vela pulsar show the glitches as discrete component of angular momentum,  $l$ , and its exchange between the observed crust and the pulsars other physical properties.<sup>5</sup> The angular momentum is transported by carriers from the superfluid core (quantized vortices of the superfluid). A continuous vortex current allows the superfluid to participate in the spindown (as the resistive elements analogous to resistive/capacitive electronic circuit), along with which continuous energy dissipation accompanies the carried angular momentum. Alpar [17] has assumed, in his study of the pulsar glitch, the resistive part of the total moment of inertia to be  $I_A$  (which may be disjoint parts with vortex density and current and may also be trapped in pinning centres).

For better understanding this is said to be similar to connected capacitor plates in an electronic circuit). These resistive parts are separated by vortex-free regions. When the capacitive charge of the vortices is discharged through this vortex free region, with a moment of inertia of  $I_B$ , without maintaining the continuous vortex current—it is called a glitch.

---

<sup>5</sup> Note that the continuous element of the angular momentum exchange with other components of the pulsar also exists.

Alpar [17] explains the extremely fast process of unpinning and repinning via movement within the regions A and B (resistive and vortex free respectively), which reduces the rate of superfluid core rotation by the amount of  $\delta\Omega$  in the region B. By assuming that the area density of the unpinned vortices is uniform in A, Alpar [17] gathers that the mean rate of decrease in superfluid core rotation for A is  $\delta\Omega/2$ , that is half of that of B.

These losses from region A and B are compensated by the gain of momentum by the pulsar's crust, which is observed through the increase of rotational speed  $\Delta\Omega$ , which is the glitch of the pulsar. This glitch is thus expressed as:

$$\delta\Omega = \frac{\frac{1}{2}I_A + I_B}{I_C} \delta\Omega \quad (7)$$

Where  $I_C$  is the effective moment of inertia [17]. The spindown rate of both the superfluid core and the crust depends on the vortex current (that is driven by rotation rates delay) that attains the internal torque for the pulsar. The lag in the rotation rate is in turn compensated by the changes in the rotation rate of the crust and superfluid core,  $\Delta\Omega$  and  $\delta\Omega$  respectively. Therefore, there is a change that is caused by the changes in the glitch in the crust's spindown rate,  $\Delta\dot{\Omega}$ . This glitch-induced change partially affects the spindown rate, which is healed exponentially (with relaxation times less than a month in the Vela pulsar); however, this affect is temporary. Permanent effect on the pulsar is on its spindown rate that changes, which does not remedy in a prompt exponential decay (unlike the temporary case), instead relaxes gradually as a time dependent linear function. This process of healing continues until similar glitches show, by the time of which the process is mostly complete [17].

$$\Delta\dot{\Omega}(t) = \Delta\dot{\Omega}(0)\left(1 - \frac{t}{t_g}\right) \quad (8)$$

The expression above shows the relationship of time dependent glitch induced change with its initial value and the parameter describing the slope of relaxation in spindown,  $t_g$ . Relationship between the parameter, spindown rates and the moment of inertia is thus expressed by Alpar [17] as:

$$t_g = \frac{\delta\Omega}{|\dot{\Omega}|} \quad (9)$$

$$\frac{\Delta\dot{\Omega}(0)}{|\dot{\Omega}|} = \frac{I_A}{I_C} \quad (10)$$

By relating the model parameters to the observed parameters, Alpar[17] interprets that, due to importance of the current function in the driving lag (which stops when the lag is compensated by the glitch), the glitch induced change in the spindown rate causes the complete halt in the flowing of the vortex current [in region A].<sup>6</sup> Following the relation,  $t_g$  for the Vela pulsar is within 20% of the time range—this means that the unpinned vortex density has enough time to be repined. Thus using Eq<sup>n</sup>. (7) to (10) second derivative of  $\Omega$  is expressed:

$$\ddot{\Omega} = \frac{I_A \dot{\Omega}^2}{I \delta \Omega} \quad (11)$$

$$\ddot{\Omega} = \left(\beta + \frac{1}{2}\right) \left[ \frac{\left(\left(\frac{\Delta\dot{\Omega}}{\dot{\Omega}}\right)_{-3}\right)^2}{\left(\frac{\Delta\dot{\Omega}}{\dot{\Omega}}\right)_{-6}} \right] \left(\frac{\dot{\Omega}^2}{\Omega}\right) \quad (12)$$

$$\text{Where } \beta = \frac{I_B}{I_A}. \quad (13)$$

The positive anomalous breaking index is then expressed as:

---

<sup>6</sup> This as per Jargon model is known as the ‘nonlinear response’.

$$\eta \equiv \frac{\dot{\Omega}}{\left(\frac{\Omega^2}{\Omega}\right)} = \left(\beta + \frac{1}{2}\right) \left[ \frac{\left(\left(\frac{\Delta\Omega}{\Omega}\right)_{-3}\right)^2}{\left(\frac{\Delta\Omega}{\Omega}\right)_{-6}} \right] \quad (14)$$

From which the time until the next glitch is calculated and thus expressed:

$$t_g = 2 \times 10^{-3} \left(\beta + \frac{1}{2}\right)^{-1} \tau_{sd} \left[ \frac{\left(\frac{\Delta\Omega}{\Omega}\right)_{-6}}{\left(\frac{\Delta\Omega}{\Omega}\right)_{-3}} \right] \quad (15)$$

Where the characteristic dipole spindown time is expressed as,

$$\tau_{sd} = \frac{\Omega}{2|\dot{\Omega}|} \quad (16)$$

Via all these calculations and assumptions Alpar [17] was able to conclude that there are two implications of this detailed study of vortex-unpinned model for Vela pulsar:

- i. The Vela pulsar is in a regime where its response is nonlinear and it is very sensitive to perturbation of lag. The energy dissipation rate is expressed as ( $\dot{E}_{dissipation}$  establishes the thermal luminosities of older NS and  $\omega$  is the lag between rotations of the crust and the repined/pinned superfluid core):<sup>7</sup>

$$\dot{E}_{dissipation} \sim I_A \omega |\dot{\Omega}| > I_A \delta\Omega |\dot{\Omega}| \sim 10^{41} |\dot{\Omega}| \text{ ergs}^{-1} \quad (17)$$

- ii. The superfluid core is strongly coupled with the outer crust (for short time) which also means that the precession would be dampened (this was determined by the relationship observed between the moment of inertias).

---

<sup>7</sup> Note that all the formulae and their derivations in section 5.2 has been taken from Alpar's article.



Given below are some relationship curves for both Vela (left) and Crab (right) to compare and understand the properties (mentioned above) of the Vela pulsar better.

**Table 2** The data used for the relationship curves are thus given

Properties	Vela pulsar	Crab
$\nu$	11 Hz	30 Hz
$\dot{\nu}$	$-1.6 \times 10^{-11} \text{ Hz/s}$	$-3.9 \times 10^{-12} \text{ Hz/s}$
Age	11000 yr	1000 yr
Number of Glitches	12	12
$\frac{\Delta V}{V}$	$\sim 10^{-6}$	$\sim 10^{-9}$

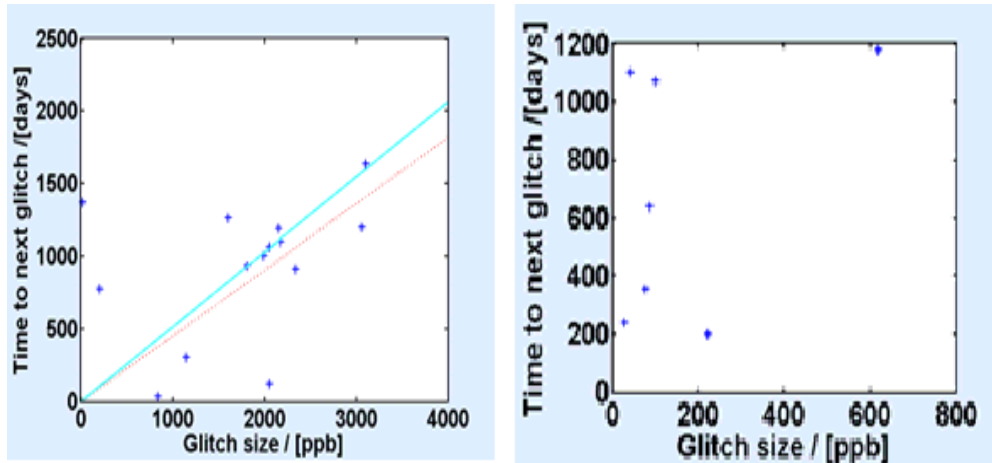


Figure 10 The relationship of the predicted time of glitch and glitch size. For Vela - The red line is the linear fit passing through origin to all data and the cyan line is the best-fitted line for the large glitches; however, no such relationship is observed for the large glitches; however no such relationship is observed for Crab [18].

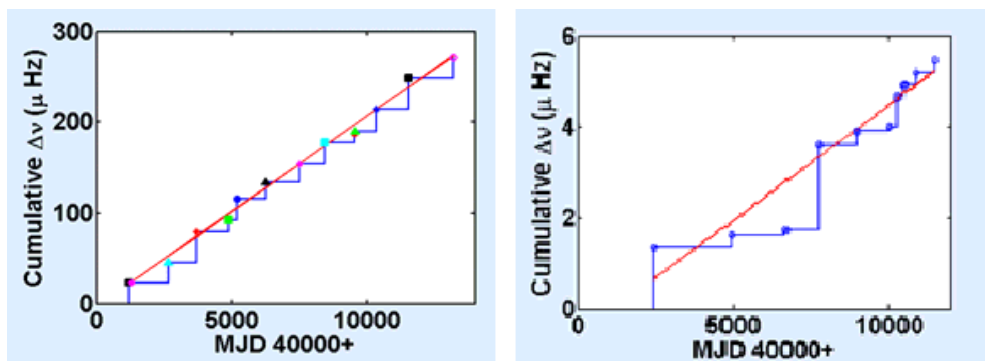


Figure 11 The sum of glitch magnitude versus time plotted for Vela and Crab. The slope gives the value of glitch activity,  $A_g$ , which for The Vela pulsar is approximately  $8 \mu\text{Hz/yr}$  [18].

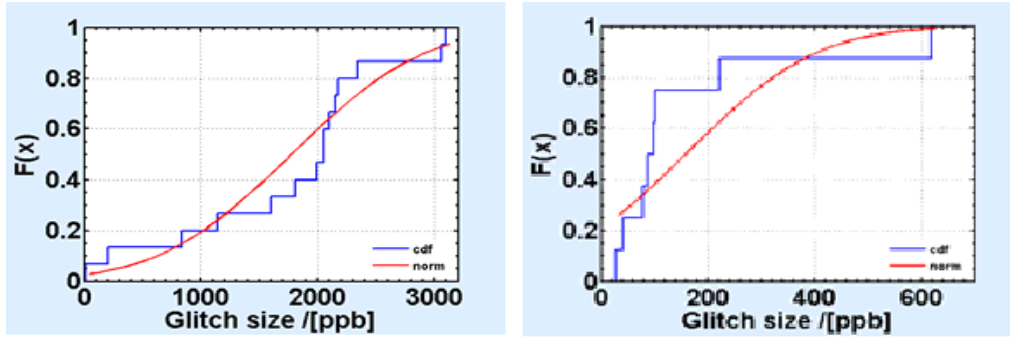


Figure 12 The plotted cumulative distribution function (cdf) and normal distribution function plotted and compared with each other [18].

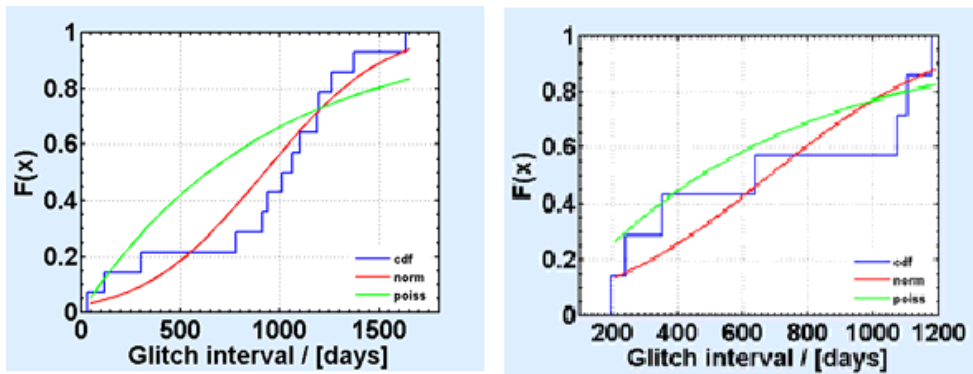


Figure 13 Comparison of the cumulative distribution function (cdf) with the normal and Poisson distribution function, enabling the determination of the conclusion, i.e. the distribution of glitches in time is not random for Vela. [18].

Negi[16] assigns  $4.1M_{\odot}$  as an upper bound to the mass of neutron star to justify his starquake model as a contender to the vortex unpinning model, which constrains the previous models; this gives Vela a glitch healing parameter  $Q \approx 0.12$  (matches previously mentioned value in 5.1), corresponding transition energy,  $E_b = 3.864 \times 10^{14} \text{ gcm}^{-3}$  [16]; thus revealing a possibility of the starquake model as the glitch generator for the Vela pulsar, (With the help of the fig 10 to 13 this remodel can also be proven as likely for the Crab. However the parallel sequence of stable neutron star mass, combination of different masses, may correspond to different values of maximum or minimum mass), in case of which the surface red shift of the pulsar corresponds to the pre-registered glitch healing parameter,  $Q \approx 0.12$  (central weighted mean value). For a lower weighted mean value of this glitch healing parameter, the red shift mass and surface decreases and for a higher weighted mean value the viewed structure changes to an ultra-compact object, UCO (entities that are not yet much known about)[16].

### **3.3 PWN study of the Vela:**

The pulsar wind nebula is studied to diagnose the spatial and spectral distribution of the high-energy electron responsible for  $\gamma$ -ray production in TeV range [18]. This production is directed by inverse Compton scattering of the cosmic background that encounter low energy photons ( $E < 0.15\text{eV}$  range) to produce secondary electrons (via  $e^+/e^-$  procedure) that in turn radiates synchrotron secondary gamma rays. The maximum value of synchrotron from secondary electron production for Vela pulsar and similar kind is  $20\text{GeV}$  [1]. With new observational data after 2008 at various angles and extended regions, a new method was used to combine the main discriminating variable factors in a single estimator to analyze and form signal to background discrimination, that allows the smallest of signals to be vastly studied [19]. This analysis,  $X_{\text{eff}}$  for the Vela X region revealed improved sensitivity for spectral analysis and showed  $\gamma$ -ray emission up to  $1.2^\circ$  from the centre (formally defined)[19]. Further study done by Dubois *et al.*[19], on a larger region than  $1.2^\circ$  from the centre of gravity shows that the energy spectrum of photons in the region is compatible with that of the gamma envelope (in terms of spectral index and high energy cut off) while the importance of integrated flux decreases by a factor of 3[19].

## CHAPTER 4: MAGNETOSPHERE OF VELA PULSAR

Takata [20] explored the already existing model that gave the solution to particles in motion under electric and radiation reaction force; they did this by considering the non-dipole field near the light cylinder due to the field lines being expected to deviate from dipole configuration. This is essentially due to the influence of the pulsar wind or the electric current. Then the position of low energy cut-off in the curvature spectrum shown—depends upon the curvature radius of the field lines near the light cylinder. They use Vela (PSR-0833-45) and another pulsar to justify this model. Both these pulsars, despite having very similar magnetospheric parameters as well as surface temperature [20], show very distinct gamma spectrum, which makes it even more eligible for the model.

Keeping the following equations in mind:

$$E = \frac{-\Omega r B}{c} = -\nabla \Phi_{co} \quad (18)$$

$$\nabla^2 \Phi_{co} = 4\pi \rho_{GJ} \quad (19)$$

$$\nabla^2 \Phi_{nco} = -4\pi \rho_{eff} \quad (20)$$

$$E_{||} = \frac{B \nabla \Phi_{nco}}{|B|} \quad (21)$$

$$\rho_{GJ} \sim \frac{\Omega B_z}{2\pi c} \quad (22)$$

Where,  $\Phi_{co}$  = *corotational potential*,  $\rho_{GJ}$  = *goldreich – Julian  $\rho$* ,  $\Phi_{nco}$  = *non – corotational potential* &  $\rho_{eff}$  = *effective  $\rho$*

If charged particles move with a velocity close to the speed of light, C along the magnetic field lines then,

$$\frac{N_{\pm}(s)}{B(s)} = \text{constant along the field line}$$

Pair production causes continuity to be:

$$\pm B \frac{d}{ds} \left( \frac{N_{\pm}}{B} \right) = \frac{i}{\cos \Psi} \int_0^{\infty} d\varepsilon_v [\eta_{p+} G_+ + \eta_{p-} G_-] \quad (23)$$

$G_{\pm}$  indicates distribution function propagation. Lorentz factor in the gap is obtained by assuming saturation of particles motion in the balance between electric and radiation reaction force.

$$\Gamma_{sat}(R_c, E_{||}) = \left( \frac{3R_c^2}{2e} E_{||} + 1 \right)^{1/4} \quad (24)$$

Unity of bracket is only influential at  $E_{||} = 0$ ,

$$\Gamma_{sat} = \Gamma, \text{ at } t_{ac} = t_d,$$

$$\Gamma > \Gamma_{sat}, \text{ at } t_{ac} > t_d$$

$$\Gamma < \Gamma_{sat}, \text{ at } t_{ac} < t_d$$

$$\text{if } t_d \ll t_{cr} \ \& \ t_{ac} \ll t_{cr} \text{ then } t_{cr} = \frac{W_{||}}{c}$$

#### **4.1 Boundary**

For  $S_1$  and  $S_2$  i.e. the inner and outer boundary;

$$E_{||}(s_1) = E_{||}(s_2) = 0$$

Assuming gamma ray does not come into the gap across either boundary

$$G_+(s_1) = G_-(s_2) = 0$$

Since current circulates magnetosphere, some particles seep through the gap at the boundaries, parameterizing the inflows:

$$j_1 = \frac{N_+(S_1)}{\frac{\Omega B(s_1)}{2\pi c}} \quad (25)$$

$$j_2 = \frac{N_-(S_2)}{\frac{\Omega B(s_2)}{2\pi c}} \quad (26)$$

Particles are injected at Goldreich-Julian rate of  $S = S_1 = S_2$  if either  $j_1$  or  $j_2$  is 0.

The current conservation per unit flux tube:

$$j_{tot} = j_1 + j_2 = \frac{N_+(S_1)}{\frac{\Omega B(s_1)}{2\pi c}} + \frac{N_-(S_2)}{\frac{\Omega B(s_2)}{2\pi c}} = \text{constant} \quad (27)$$

$$\therefore j_{tot} = j_1 + j_2 + j_g, \text{ where } j_g \text{ is the } j \text{ for gap} \quad (28)$$



## CHAPTER 5: PULSAR MAGNETOSPHERE ELECTRODYNAMICS

Since pulsar magnetosphere's dynamics is related to and found through the electron-positron pair production plasma, Maxwell equations for E and B are introduced:

$$\text{div } E = 4\pi\rho_e \quad (29)$$

$$\text{rot } E = -\frac{1}{c}\frac{\partial B}{\partial t} \quad (30)$$

$$\text{rot } B = \frac{4\pi}{c}j + \frac{1}{c}\frac{\partial E}{\partial t} \quad (31)$$

$$\text{div } B = 0 \quad (32)$$

$$q = \frac{\partial F^\pm}{\partial t} + Bv_\parallel \frac{\partial}{\partial r_\parallel} \left( \frac{F^\pm}{B} \right) \pm \frac{e}{B} BE \frac{\partial F^\pm}{\partial p_\parallel} + v_\perp \frac{\partial F^\pm}{\partial r_\perp} \quad (33)$$

Here  $F^\mp$  is distribution function of electron and positron,  $r_\parallel$  is the coordinate along magnetic field line, and  $r_\perp$  is the orthogonal coordinate.

$$\rho_e = e(n^+ - n^-) \quad (34)$$

$$j_e = e(n^+v^+ - n^-v^-) \quad (35)$$

$$r_\parallel = \frac{cp_\parallel}{\sqrt{p_\parallel^2 + m^2c^2}} \quad (36)$$

Where  $\rho_e$  is charge density,  $j_e$  is current density,  $n^\pm$  is particle concentration,  $v^\pm$  is the mean velocity of the particle.

$$n^\pm = \int F^\pm dp_\parallel \quad (37)$$

$$n^\pm v^\pm_\parallel = \frac{1}{m_e} \int \frac{p_\parallel F^\pm}{v} dp_\parallel \quad (38)$$

$$p_\perp = m_e v v_\perp \quad (39)$$

$$v = \sqrt{1 + \frac{p_{\parallel}^2 + p_{\perp}^2}{m_e^2 c^2}} \quad (40)$$

$m_e$  is the rest mass energy,  $v$  is the Lorentz factor,  $p_{\perp}$  is the transverse moment of particles.

$$\frac{\partial p_{\perp}}{\partial t} + (v_{\perp} \nabla) p_{\perp} \mp e \left[ E_{\perp} + \frac{1}{m_e v c} (p_{\perp} B) \right] = 0 \quad (41)$$

Assuming no thermal energy dispersion in  $p_{\perp}$ , the real conditions in a pulsar magnetosphere is corresponded. This is connected with rapid loss of  $p_{\perp}$  either by the particles, electron or proton in a strong magnetic field due to synchrotron radiation, that has a duration  $\tau_r$  and is expressed thus:

$$\tau_r \cong \frac{4 \times 10^{-16} v}{B_{12}^2} \text{ s}, \text{ where } B_{12} = B 10^{-12} G^{-1} \quad (42)$$

## CHAPTER 6: EXPLORING VELA PULSAR MAGNETOSPHERE

### 6.1 X-ray field:

Soft photon field for pair creation rate  $np_{\pm}\sigma_p$  is maxima at soft X-ray band. These X-rays (observed) are dominated in the Vela pulsar by surface black body radiation. Taking only surface black body radiation as soft photon field—photon number density between energies  $m_e c^2 E_x$  and  $m_e v c(E_x + dE_x)$  is:

$$\frac{dN_x}{dE_x} = \frac{1}{4\pi} \left( \frac{2m_e \pi c^2}{ch} \right)^3 \left( \frac{A_s}{4\pi r^2} \right) \left( \frac{E_x^2}{e^{\left( \frac{m_e c^2 E_x}{KT_s} \right) - 1}} \right) \quad (43)$$

$A_s \rightarrow$  observed emitting area and  $KT_s \rightarrow$  surface temperature

These are used to calculate the pair production rate at each point, where collision angle  $\mu_c$  is:

$$\mu_c = \cos \Phi_v \chi \sin \theta; \quad (44)$$

$$\Phi_v \chi = \sin^{-1} \left( r \sin \frac{\theta \Omega}{c} \right) \quad (45)$$

### 6.2 Curvature radiation-outside the gap:

Since  $\Gamma_{sat} \propto \sqrt[4]{E_{\parallel}}$ ,  $\Gamma_{sat}$  does not change significantly in the gap; boundaries however are exceptions. Therefore, producing a curvature spectrum that is analogous to the one produced by mono-energetic particles.

For  $t_{ac} = t_d$ ; they become longer near boundaries compared to  $t_{cr}$ . Their ratio therefore stands thus:

$$\frac{t_d}{t_{cr}} \sim \frac{3}{2} \frac{m_e c^2}{e^2} \frac{R_c^2}{\Gamma^3} W_{\parallel}^{-1} \quad (46)$$

The particles escape the gap with large  $\Gamma_{out} \sim 10^7$  range and radiate  $\gamma$ -rays outside the gap as well. Since particles simply lose energy by radiation after leaving the gap due to  $E_{\parallel}$  being screened out.  $\Gamma_{out}$  then decreases:

$$\frac{d\Gamma(s)}{ds} = -\frac{2}{3} \frac{e^2 \Gamma^4(s)}{m_e c^2 R_c^2(s)} \quad (47)$$

$\Gamma$  per unit length decreases at a proportional rate to  $\Gamma^4(s)$  if  $R_c$  is constant.

$$\frac{dN_e(\Gamma)}{d\Gamma} \propto \Gamma^{-4} \quad (48)$$

Therefore, low power  $\gamma$ -ray spectrum is found by curvature radiation superposition at various positions.

By the following equation, we get the photon index,  $p$ :

$$p = \frac{5}{3} \text{ for } E_v < E_{out}$$

$E_{out} = \frac{3h}{4\pi} \frac{\Gamma_{out}^3 c}{R_c}$ , which is the critical energy for highest energy particles.

$$E_{min} = \frac{3h}{4\pi} \frac{\Gamma_{min}^3 c}{R_c}$$

Below  $E_{min}$ ,  $p = \frac{2}{3}$

For Vela pulsar  $E_{min} \sim 80 \text{ MeV}$ ,  $\Gamma \sim 8 \cdot 10^6$

It is assumed the spectrum improves between  $E_{out}$  and  $E_{min}$ . Pair creation cascades as a result of  $e^{\pm}$  conversion by  $\nu B \rightarrow e^{\pm} B$  and comes from  $\gamma$ -ray radiated toward the star. This cascaded pair [20& all ref. therein], has  $p \sim 1.9$  in X-ray region. This spectral index is consistent for Vela.

### **6.3 The electric structure:**

Takata [20] calculates  $E_{\parallel}$  for Vela pulsar, the model parameters for which being:

$$(j_{tot}, j_1, j_2) = (0.201, 0.191, 0.001) \& \alpha_{in} = 45^\circ$$

Plotting a distance (along the field lines) versus electric field, they show that the gap width  $W_{\parallel}$  is shorter than  $W_{lc} = 4.25 \times 10^8 \text{ cm}$ .  $W_{\parallel}$  differentiated by the mean free path for pair creation, this is shorter [20], explains due to the gap being filled with abundant  $\gamma$ -rays and X-rays. The graph also shows  $E_{\parallel}$  of Vela increases until certain  $\rho_{GJ}$  with  $W_{\parallel}$  increase.

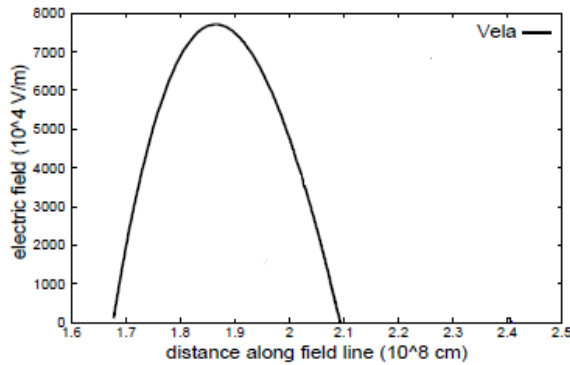


**Figure 14 Distance (along the field lines) versus electric field.**

#### **6.4 Gamma-ray spectrum:**

Takata [20] uses dimensionless current parameters for Vela to plot an EGRET phase average spectrum.<sup>8</sup> From this they determine that the spectrum from outside the gap appears between  $E_{out}$  to  $E_{min}$ , 1GeV to 80MeV,  $p \sim \frac{5}{3}$  and  $p \sim \frac{2}{3}$  below  $E_{min}$ , which agrees with the previous conclusion. Although the calculated data is different (slightly) than the EGRET data, which is due to assumption made about motion saturation of particles at equilibrium  $\Gamma$ , a better suited result, they conclude, may be possible in absence of the assumption.

<sup>8</sup> EGRET—Energetic Gamma-Ray Experiment Telescope (full forms, <http://fullformplus.com/98294/EGRET/>)

### **6.5 Spectral dependence on the curvature of field line:**

Considering Vela field line parameters, the field lines appear to be depending around spectra of 100MeV. In case of stretched lines, curvature contributes very little to the spectrum—due to less efficient curvature emission, i.e. particles in a dipole escaping with minimum energy compared to light cylinder. This is why stretched field lines have greater  $E_{min}$  than un-stretched.

## CHAPTER 7: GVARAMADZE'S STUDY ON THE VELA PULSAR

### 7.1 Velocity of Vela pulsar:

Gvaramadze [21] explains the relationship of Vela pulsar's velocity with its distance. Initial assumptions of the area of the SNR created some problems in this estimation that however was later dissolved since the SNR extended far beyond its visible area—tactically placing the pulsar at its core (shown in the fig.15) and proving the relationship of its velocity with distance legit. Gvaramadze [21] mentions a radio filament that is projected on the Vela pulsar, which is actually a large-scale deformation of the Vela SNR,'s (when its shell is viewed edge-on); this deformation itself has a significant transverse velocity. Assuming that the deformation lies on the approaching side of the Vela SNR's shell, he suggested that the turbulent material associated with the shell deformation is responsible for the scattering of the Vela pulsar.<sup>9</sup>From the suggested scintillations and proper motion velocities, he [21] concludes that the phenomenon proposed [ 14, 21 and ref. therein], for the value  $x = 1.5 (D/1.5 \text{ kpc})^{-1}$ ,  $v_{\text{iss}} = 186 \text{ kms}^{-1}$  is obtained, for which the possibility of the transverse velocity being balanced is probable.

---

<sup>9</sup> It should be noted that Gvaramadze's hypothesis was based on various scintillation and proper motion velocity equations- that all had a certain percentage of error in calculation, causing the conclusion to be trial error based.

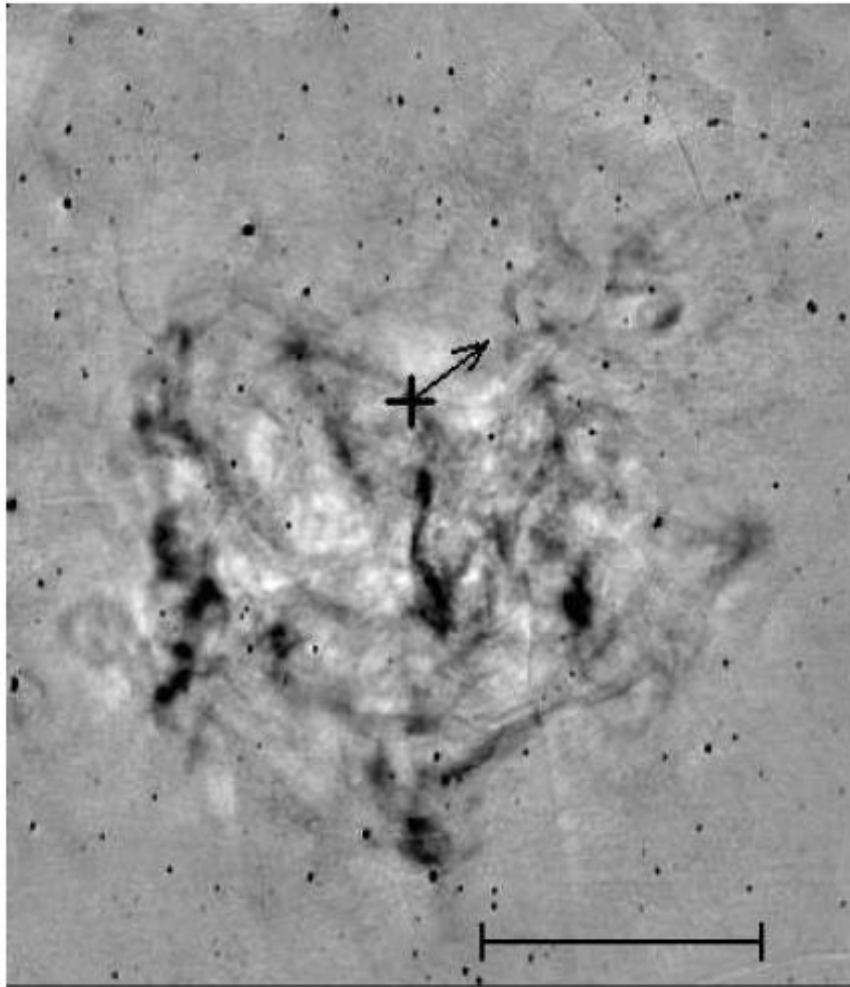


Figure 15 843 MHz image of the central part of the Vela SNR, the position of the Vela pulsar is indicated by the cross mark. The arrow attached to it shows the direction of the pulsar proper motion velocity [21]



## DISCUSSION

The Vela pulsar shows excessive variation in its characteristics. Its magnetosphere in itself has shown variety of characteristics that no other pulsar has shown so far. The Vela pulsars glitches are so divergent that neither the starquake model nor the Vortex unpinning model is completely applicable to it. The same argument is also valid for the pulsars dynamics—neither the helical structure precession nor the kink magneto-hydrodynamic instability fully explains the jet and helical behaviour. All the recent studies show how Vela pulsar has similarities with other pulsars such as: pulsar (PSR B0329+54), an optical pulsar (the Crab pulsar, PSR B0531+21), an old millisecond pulsar (PSR J0437-4715) and the 2<sup>nd</sup> fastest known pulsar (PSR B1937+21), despite which the Vela pulsar can be characterized as none of the kinds mentioned. It is only valid to conclude that further study is required to fully understand and propose a perfect model that applies to this particular pulsar and any of its kind that may be discovered in the future.

## BIBLIOGRAPHY

- [1] Mofiz, A. U., & Bhattacharya, D. (2007). On gamma-ray emission from pulsar magnetosphere. *4*.
- [2] Rishbeth, H. (December 1958). "Radio Emission from the Vela-Puppis Region". *Australian Journal of Physics***11** (4): 550–563.  
Bibcode:1958AuJPh..11..550R. doi:10.1071/PH580550.
- [3] Grondin, M. H., Romani, R. W., Lemoine-Goumard, M., Guillemot, L., Harding, A. K., & Reposeur, T. (2013, July 20). THE VELA–X PULSAR WIND NEBULA REVISITED WITH 4 YEARS OF FERMI LARGE AREA TELESCOPE. *Astrophysical Journal*.
- [4] Aschenbach, B., Egger, R., & Trumper, J. *Nature*, 373, 587 1995.
- [5] Large, M. I., Vaughan, A. E., and Mills, B. Y. 1968. A pulsar supernova association. *Nature*, **220**, 340-341.
- [6] Thompson, A. R., 1999. Synthesis Imaging in Radio Astronomy II, A Collection of Lectures from the Sixth NRAO/NMIMT Synthesis Imaging Summer School. ASP Conference Series, **180**, 11.
- [7] Wallace, P. T., Peterson, B. A., Murdin, P. G. *et al.* 1977. Detection of optical pulses from the Vela Pulsar. *Nature*, **266**, 692-694.
- [8] Ogelman, H., Orío, M., Krautter, J., Starrfield, S., 1993, *Nature*, 361, 331.
- [9] Lyne, A. G., & Graham-Smith, F. (2012). *Pulsar Astronomy*. Cambridge University Press.

- [10] Romani, R. W., Kargaltsev, O., Pavlov, G. G. "The Vela Pulsar in the Ultraviolet"  
*The Astrophysical Journal* 627:383-389, 1<sup>st</sup> July 2005.
- [11] Shibano, Yu. A., Koptsevich, A. B., Sollerman, J., & Lundquist, P. 2003, *A&A*, 406, 645.
- [12] Durant, M., Kargaltsev, O., Pavlov, G. G., Kropotina, J., & Kseniya, L. (2012, Nov 2). *The helical jet of the Vela Pulsar*. Retrieved 2014, from [www.arXiv:1211.0347v1](http://www.arXiv:1211.0347v1)
- [13] European Pulsar network. Retrieved 22<sup>nd</sup> March 2014.
- [14] Camilo, F. et al. 2002a, *ApJ*, 567, L71
- [15] Morii, N. d
- [16] Negi, P. S. (2006). A starquake model for the Vela pulsar. *366*, 73-78.
- [17] Alpar, M. A. (2001, Dec 13). *Pulsar Glitch Behaviour and ZXP, SGRs and DTNs*, 1. Retrieved 2014, from [www.arXiv:astro-ph/0112306v1](http://www.arXiv:astro-ph/0112306v1)
- [18] Buchner, Sarah. Flanagan, Claire. (2011). *On the Present and Future of Pulsar Astronomy*. Retrieved 2014, from Max-Planck-Institut für extraterrestrische Physik (MPE): [www2011.mpe.mpg.de/IAU\\_JD02/poster/JD02-66.pdf](http://www2011.mpe.mpg.de/IAU_JD02/poster/JD02-66.pdf)
- [19] Dubois, F., Gluck, B., de Jager, C. O., Hinton, J., Khelifi, B., Lamanna, G., et al. (2009). *H.E.S.S. observation of the Vela X nebula*. Retrieved 2014, from [https://www.mpi-hd.mpg.de/.../2009-05-26\\_icrc0641\\_HESS\\_VelaX.pdf](https://www.mpi-hd.mpg.de/.../2009-05-26_icrc0641_HESS_VelaX.pdf)

[20] Takata, J., Shibata, S., Hirokuni, K. (2003). Outer Magnetospheric Model for Vela-like Pulsars: Formation of Sub-GeV Spectrum. Retrieved 2014, from [www.arxiv:astro-ph/0312010v1](http://www.arxiv.org/abs/astro-ph/0312010v1)

[21] Gvaramadze, V. (2001, Jan 22). *On the velocity of the Vela Pulsar*. Retrieved 2014, from [www.arXiv:astro-ph/0005580v3](http://www.arxiv.org/abs/astro-ph/0005580v3)